

# Sliding ferroelectric control of unconventional magnetism in stacked bilayers

Yongqian Zhu,<sup>1,2</sup> Mingqiang Gu,<sup>3</sup> Yuntian Liu,<sup>3</sup> Xiaobing Chen,<sup>3,4</sup> Yuhui Li,<sup>3</sup> Shixuan Du,<sup>1,2,5,\*</sup> and Qihang Liu<sup>3,4,†</sup>

<sup>1</sup>*Beijing National Laboratory for Condensed Matter Physics,  
Institute of Physics, Chinese Academy of Sciences, Beijing 100190, China*

<sup>2</sup>*University of Chinese Academy of Sciences, Chinese Academy of Sciences, Beijing 100190, China*

<sup>3</sup>*Department of Physics and Guangdong Basic Research Center of Excellence for Quantum Science,  
Southern University of Science and Technology, Shenzhen 518055, China*

<sup>4</sup>*China Quantum Science Center of Guangdong-Hong Kong-Macao Greater Bay Area (Guangdong), Shenzhen 518045, China*

<sup>5</sup>*Songshan Lake Materials Laboratory, Dongguan 523808, China*

The control of unconventional magnetism, which displays an antiferromagnetic configuration with ferromagnetism-like properties, has drawn intense attention for advancing antiferromagnetic spintronics. Here, through symmetry analysis, we propose a general stacking rule, characterized by a connection operator linking two stacked bilayers, for controlling unconventional magnetism via sliding ferroelectricity. Such rule enables the simultaneous switching of both electric polarization and nonrelativistic spin splitting or anomalous Hall effect in altermagnets, a class of collinear unconventional magnets. By comprehensively surveying the 80 layer groups, we identify all the stacking orders that allow for such two types of simultaneous switching. Combined with first-principles calculations, we demonstrate the sliding ferroelectric control of spin polarization and anomalous Hall effect in the altermagnetic AgF<sub>2</sub> bilayer. Our work provides a symmetry strategy for achieving ferroelectric control of unconventional magnetism in bilayer systems and opens avenues for exploring new types of magnetoelectric coupling.

*Introduction*—Unconventional magnetism is broadly characterized by an antiferromagnetic (AFM) configuration yet exhibiting ferromagnetism-like (FM-like) properties, including spin splitting, anomalous Hall effect (AHE), quantum geometry, topological magnons, etc [1]. Recent advances in classifying unconventional magnets according to spin-group symmetry have expanded the current understanding of magnetism [2–10]. A prominent example is altermagnetism, a type of collinear AFM that displays nonrelativistic spin splitting in momentum space [3, 4, 11–15]. The spin splitting originates from the collinear magnetic order rather than from relativistic spin-orbit coupling (SOC). Such magnetic order-induced spin polarization enables various spintronic applications, such as spin-polarized currents, spin-to-charge conversion, spin torques, and magnetoresistance [4, 12, 16–22]. Another representative category of unconventional magnetism is the AFM exhibiting the anomalous Hall effect (AHE) [23–28], which enables the electrical read-out of the magnetic state. In collinear and coplanar AFMs, the occurrence of the AHE necessarily requires SOC, while for noncoplanar AFM, it can originate solely from the magnetic order [29].

In AFM memories, controlling the two key properties of unconventional magnetism, spin splitting and AHE, opens new possibilities for information writing [30, 31]. A typical approach involves manipulating AFM moments by a spin torque, which requires electrical current and thus suffers from large energy dissipation [30, 32, 33]. Sliding ferroelectricity provides an energy-efficient alternative way [34–36] for controlling unconventional magnetism through a gate voltage, e.g., switching the spin polarization in altermagnets [37]. However, a universal and efficient strategy for designing materials with coupled

sliding ferroelectricity and unconventional magnetism is still lacking. Stacking has been previously demonstrated as an effective approach for inducing either sliding ferroelectricity or altermagnetism in a wide range of two-dimensional (2D) materials [38–43]. These findings motivate us to explore a general stacking strategy for achieving ferroelectric *control* of unconventional magnetism.

In this Letter, we propose a general symmetry rule for controlling unconventional magnetism via sliding ferroelectricity in bilayer systems. Such a symmetry rule can easily predict whether electric polarization and unconventional magnetism are coupled in stacked bilayers, based solely on the crystallographic layer group of their constituent monolayers, the stacking operation and the magnetic configurations of the bilayers. By applying to 80 layer groups, we identify all the stacking orders that enable ferroelectric control of spin polarization or anomalous Hall effect in altermagnetic bilayers. Combined with first-principles calculations, we demonstrate the sliding-induced simultaneous control of ferroelectricity and unconventional magnetism in altermagnetic AgF<sub>2</sub> bilayer.

*Symmetry rules for sliding ferroelectricity*—For stacked bilayers, the existence of spontaneous electric polarization or unconventional magnetism is theoretically governed by their symmetries established on different group frameworks [39, 41, 44–47]. The switching of these properties between two bilayer configurations is determined by an operator that connects them [15, 48–50], referred to as the connection operator. Obviously, the connection operator determines the coupling of ferroelectricity and unconventional magnetism. Based on these symmetry rules, we identify ferroelectric bilayers that can control unconventional magnetism as follows.

We first screen out all the stacked bilayers with sliding ferroelectricity across all 80 layer groups. A bilayer system ( $B$ ) consisting of a bottom layer ( $S$ ) and a top layer ( $S'$ ) can be expressed as  $B = S + S' = S + \hat{O}S$ , where  $\hat{O} = \{O|\mathbf{t}_o\}$  is a stacking operator transforming  $S$  into  $S'$  [39]. Here,  $O$  is the rotational part, and  $\mathbf{t}_o$  is the translational part. A stacking operator  $\hat{O}$  specifies a stacking order. We then consider a ferroelectric bilayer with the same lateral unit cell size as its constituent monolayers, possessing an out-of-plane electric polarization component ( $P$ ). The symmetry operator ( $\hat{R}$ ) of a bilayer system and the connection operator ( $\hat{N}$ ) between two bilayer systems [see Fig. 1(a)] can be divided into two classes,  $\hat{Q}^-$  and  $\hat{Q}^+$  ( $\hat{Q} = \hat{R}, \hat{N}$ ), which can and cannot reverse  $P$ , respectively. For each layer group of the constituent monolayer, we identify all the stacking orders with only  $\hat{R}^+$  symmetries that permit  $P$  [39]. Then, we further screen out those with switchable  $P$  through interlayer sliding (i.e., sliding ferroelectricity). For two bilayer configurations, opposite  $P$  requires a connection operator  $\hat{N} = \hat{N}^-$ , as shown in Fig. 1. By solving the equation set for  $\hat{N}^-$  across 80 layer groups, we identify all the stacking orders with switchable  $P$ , as detailed in Sec. 1 of the Supplemental Material [51]. Table I presents an example for layer groups No. 14-18 of the monolayer. A bilayer permits  $P$  when stacked with  $O = m_{001}$  and  $\mathbf{t}_o$  along the high symmetry line GB or CA.  $P$  can be switched when changing the stacking order from  $\mathbf{t}_o$  to  $-N\mathbf{t}_o + \mathbf{t}_o$  through interlayer sliding, where  $\mathbf{t}_o$  represents the pure translational symmetry of the constituent monolayer.

*Sliding ferroelectric control of spin polarization*—Having obtained all stacked bilayers with switchable  $P$ , we turn to identify those with coupled ferroelectricity and unconventional magnetism. We first consider ferroelectric control of spin polarization in altermagnets. For 2D altermagnets, the symmetry  $\hat{R}$ , that connects two sublattices with opposite spins, cannot be a translation  $\mathbf{t}$ ,

TABLE I. Stacking configuration of layer groups No. 14-18 for the sliding ferroelectric control of spin polarization and AHE.  $G_S$  ( $G_B$ ) denotes the layer group of the monolayer (bilayer);  $p2/m11$  and  $p2_1/m11$  in  $G_S$  correspond to  $pm11$  in  $G_B$ ,  $p2/b11$  and  $p2_1/b11$  in  $G_S$  correspond to  $pb11$  in  $G_B$ , and  $c2/m11$  in  $G_S$  corresponds to  $cm11$  in  $G_B$ .  $\mathbf{t}_o$  is represented by high symmetry lines  $GB$  and  $CA$  in the rectangular lattice, with  $G = (0, 0)$ ,  $A = (\frac{1}{2}, 0)$ ,  $B = (0, \frac{1}{2})$  and  $C = (\frac{1}{2}, \frac{1}{2})$ . For  $N_s^-$  ( $N_m^-$ ), only the operators capable of switching the spin polarization (AHE) are listed. The candidate monolayers are screened from Ref. [52].

$G_S$ (No.)	$\{O \mathbf{t}_o\}$	$G_B$	$N^-$	$N_s^-$	$N_m^-$	Candidates
$p2/m11(14)$						
$p2_1/m11(15)$		$pm11$	$m_{001}$	$\{2_\perp    m_{001}\}$	$m'_{001}$	$\text{AgF}_2, \text{RuF}_4$
$p2/b11(16)$	$\{m_{001} GB, CA\}$	$pb11$	$2_{010}$	$\{1  2_{010}\}$	$2_{010}$	$\text{VF}_4, \text{OsF}_4$
$p2_1/b11(17)$		$cm11$				
$c2/m11(18)$						

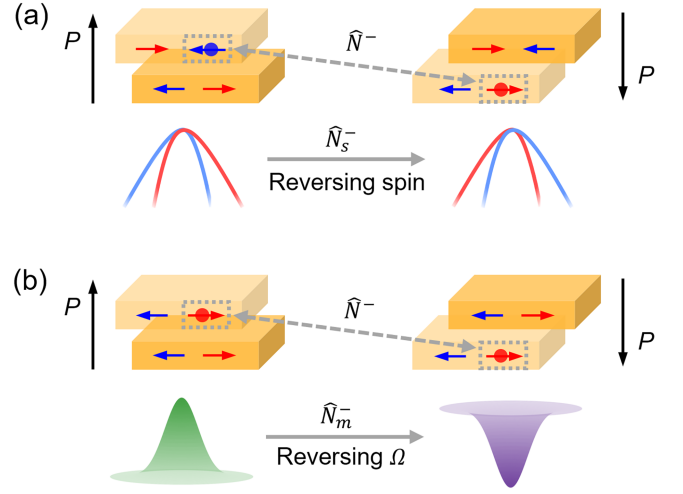


FIG. 1. Schematic diagrams of (a) configurations (upper) and bands (lower), (b) configurations (upper) and Berry curvatures (lower) of ferroelectric altermagnetic bilayers. The red and blue colors of arrows (lines) denote the opposite magnetic moments (spins). The black arrow denotes  $P$ . For the two stacked bilayers in (a) or (b), one can be transformed into the other through interlayer sliding. The sliding is equivalent to applying a  $\hat{N}^-$  transformation, which maps the top (bottom) layer of one bilayer to the bottom (top) layer of the other. The solid circles in grey dotted line boxes denote atoms connected by  $\hat{N}^-$ , which have opposite spins in (a) while the same spin in (b).

inversion  $\bar{1}$ , rotation  $2_{001}$ , or any of their combinations [40, 52, 53]. Because the considered ferroelectric bilayer contains only  $\hat{R}^+$  symmetry, the requirement is reduced to  $\hat{R}$  not being  $\mathbf{t}$ ,  $2_{001}$  or their combinations. For example, altermagnetism is allowed in the ferroelectric bilayer with layer group  $pb11$  (see Table I). Thus, we identify all the stacking orders allowing for altermagnetism from screened ferroelectric bilayers, as highlighted in Tables S1-S3 of the Supplemental Material [51]. It is worth noting that the ferroelectric altermagnetic bilayers discussed here are fundamentally different from previously reported altermagnetic bilayers with  $\hat{R} = \hat{R}^-$  (e.g., A-type AFM) [41–43], where  $\hat{R}^-$  enforces a vanishing  $P$ . In contrast, the  $\hat{R}^+$  symmetry in a bilayer system considered here originates from the constituent monolayer, a collinear antiferromagnet with different sublattices connected by  $\hat{R}^+$ .

Then, we further identify the ferroelectric altermagnetic bilayers with switchable spin polarization. We introduce the connection operator  $\hat{N}_s^-$  [Fig. 1(a)], which is an operator of the spin space group [2, 3, 5–7]. The interlayer magnetic coupling includes two types: the Néel vectors of the two constituent monolayers are aligned in the opposite or the same direction [Figs. 1(a) and 1(b)]. We assume that the collinear magnetic moment of each ion remains unchanged under interlayer sliding. Con-

sequently, for the two atoms with opposite spins connected by  $\tilde{N}^-$  [Fig. 1(a)], considering spin rotation, they are connected by  $\hat{N}_s^-$ , where the rotational part is given by  $N_s^- = \{2_\perp || N^-\}$ . Here the  $2_\perp$  indicates a twofold spin rotation along the axis perpendicular to the collinear magnetic moments. Under  $N_s^- = \{2_\perp || N^-\}$  operation, the spin polarization distribution with respect to the momentum  $s^I(\mathbf{k})$  transforms into  $s^{II}(\mathbf{k}) = N_s^- s^I(\mathbf{k}) = -s^I((N^-)^{-1}\mathbf{k})$ , where the superscripts I and II denote the two ferroelectric states connected by  $\hat{N}_s^-$ . Taking  $N^- = m_{001}$  as an example, since  $(m_{001})^{-1}\mathbf{k} = \mathbf{k}$  for any  $\mathbf{k}$  point, the spin polarization across the entire Brillouin zone can be reversed under ferroelectric switching, i.e.,  $s^{II}(\mathbf{k}) = -s^I(\mathbf{k})$ , as shown in Fig. 1(a) and Table I. Consequently, the connection operator  $N_s^-$ , which depends on  $N^-$  and the type of interlayer magnetic coupling, determines the spin polarization reversal. We find that for all the ferroelectric altermagnetic bilayers connected by  $N^-$  screened above, at least one type of interlayer magnetic coupling enables spin polarization reversal under ferroelectric switching.

*Sliding ferroelectric control of anomalous Hall effect—* Now we discuss the ferroelectric control of another facet of unconventional magnetism, i.e., AHE in AFM. Distinct from spin splitting, the symmetry requirement for AHE in 2D systems is that the sign of Berry curvature ( $\Omega$ ) remains unchanged under any symmetry operation. We consider AHE in 2D altermagnets, indicating the necessity of SOC and the framework of magnetic group, a specific subgroup of spin group. To achieve AHE in antiferromagnets with symmetry-enforced zero magnetization, the magnetic configuration must not align along the out-of-plane direction, otherwise the symmetry operations connecting the opposite-spin sublattices will reverse the sign of Berry curvature and thus enforce a zero anomalous Hall conductivity [54]. We consider the in-plane magnetic configuration. Because  $2_{001}$  symmetry of a 2D altermagnet only connects the same-spin sublattice, it will result in a  $2'_{001}$  symmetry in the magnetic point group for the in-plane configuration, leading to a vanishing AHE. Hence, any altermagnetic bilayers with  $2_{001}$  point-group symmetry should be ruled out. We screen out all the stacking orders permitting AHE from the ferroelectric altermagnetic bilayers, as highlighted in Tables S1-S3 of the Supplemental Material [51].

We further identify ferroelectric altermagnetic bilayers with controllable AHE, which requires a sign reversal of Berry curvature under ferroelectric switching [see Fig. 1(b)]. When considering SOC, the connection operator belongs to magnetic space groups and is denoted as  $\tilde{N}_m^-$ . The collinear in-plane magnetic configuration imposes a constraint that  $N_m^- \in \{m_{001}, m'_{001}, 2_\alpha, 2'_\alpha\}$ , indicating that  $N^- \in \{m_{001}, 2_\alpha\}$ , where  $2_\alpha$  denotes a twofold rotation with the rotational axis along in-plane  $\alpha$  direction. The sign reversal of Berry curvature requires

$N_m^- \in \{m'_{001}, 2_\alpha\}$  (see Table I). This condition can be satisfied for all the above-screened ferroelectric altermagnetic bilayers with AHE under an appropriate magnetic configuration. Specifically,  $N_m^- = m'_{001}$  requires that the two atoms connected by  $N^- = m_{001}$  have the same spin [see Fig. 1(b)]. On the other hand,  $N_m^- = 2_\alpha$  requires the two atoms connected by  $N^- = 2_\alpha$  have the same (opposite) spins when the spin is parallel (perpendicular) to the rotational axis of  $2_\alpha$ .

It is worth noting that AHE switching is not necessarily accompanied by a spin polarization switching in momentum space. According to our symmetry rules, for the stacking orders connected only by  $N^- = 2_\alpha$ , AHE and spin polarization can be switched simultaneously under ferroelectric switching. We mark all the stacking orders that allow for a simultaneous ferroelectric switching of both AHE and spin polarization, as highlighted in Tables S1-S3 of the Supplemental Material [51].

*Sliding ferroelectric control of unconventional magnetism in altermagnetic bilayer  $\text{AgF}_2$ —*We now apply the above symmetry analysis to realistic materials. Monolayer candidate materials that enable ferroelectric control of spin polarization and AHE via bilayer stacking are listed in Table I and Tables S1-S3 of the Supplemental Material [51]. As an example, we consider  $\text{AgF}_2$ , whose bulk phase has been synthesized experimentally [55, 56]. Monolayer  $\text{AgF}_2$  is a  $d$ -wave altermagnetic candidate with the crystallographic layer group  $p2_1/b11$  (No. 17) [22, 52]. The sublattices with opposite spins are connected by symmetries  $\{m_{100}|\frac{1}{2}, \frac{1}{2}\}$  and  $\{2_{100}|\frac{1}{2}, \frac{1}{2}\}$ . Although ferroelectricity is prohibited in monolayer  $\text{AgF}_2$  due to the inversion symmetry, according to Table I, a bilayer configuration allows for ferroelectric control of spin polarization and AHE when it is stacked with  $O = m_{001}$  and  $t_o$  along the high symmetry line GB or CA.

We next perform density functional theory (DFT) calculations on bilayer  $\text{AgF}_2$ . As shown in Fig. 2(a), the two energy minima with different translations  $t_{o1}$  (0.5, -0.16) and  $t_{o2}$  (0.5, 0.16) denote the ground states of stacked  $\text{AgF}_2$  bilayers. We denote these two bilayer configurations as  $B_1$  and  $B_2$ , which are stacked with  $\hat{O}_1 = \{m_{001}|(0.5, -0.16)\}$  and  $\hat{O}_2 = \{m_{001}|(0.5, 0.16)\}$  respectively, as shown in Fig. 2(b). Their interlayer magnetic coupling includes two types: type-I and type-II, as shown in the insets of Figs. 2(c) and 3(a), respectively. DFT calculations show that type-I is the magnetic ground state, with an energy 0.26 meV/f.u. lower than that of type-II. The stacking breaks inversion symmetry and transforms the layer group  $p2_1/b11$  of the monolayer into  $pb11$  of the bilayer, inducing a polarization  $P$  in  $B_1$  ( $B_2$ ) configuration [see Fig. 2(c)].  $B_1$  and  $B_2$  are connected by  $N^- = m_{001}$ , enforcing exactly opposite  $P$  with the same amplitude (1.66 pC/m) for  $B_1$  and  $B_2$  configurations. We consider the sliding path between  $B_1$  and  $B_2$  shown in Fig. 2(a), where the intermediate state, located at the midpoint  $t_{o0} = (0.5, 0)$ , is stacked by

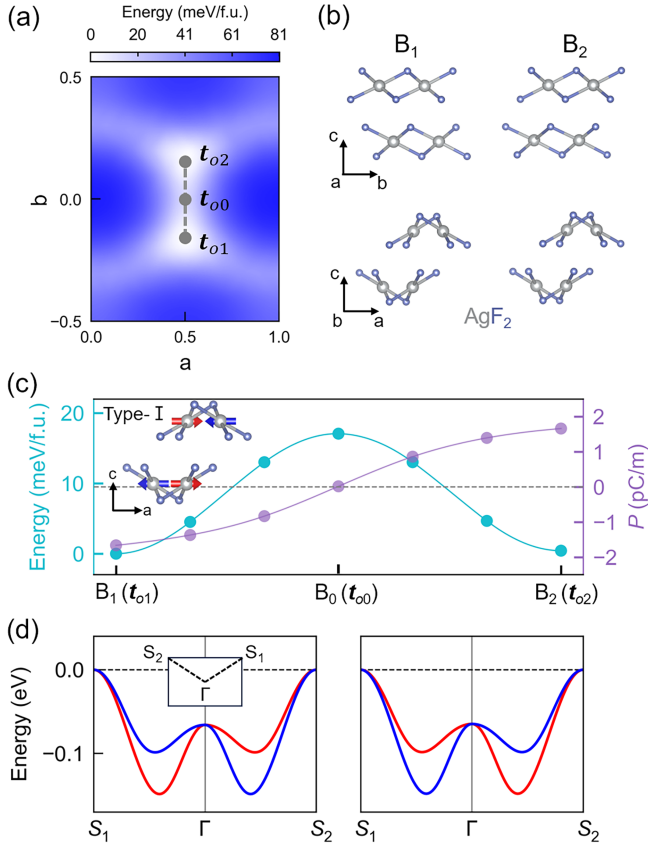


FIG. 2. (a) Energy distribution of AgF<sub>2</sub> bilayers stacked with the same  $O = m_{001}$  but different translations, with the ground state energy as the reference. The ground states are located at points  $\mathbf{t}_{o1}$  (0.5, -0.16) and  $\mathbf{t}_{o2}$  (0.5, 0.16). The gray dotted line between  $\mathbf{t}_{o1}$  and  $\mathbf{t}_{o2}$  denotes the ferroelectric switching path, with the midpoint  $\mathbf{t}_{o0}$  (0.5, 0). The bilayers located at  $\mathbf{t}_{o0}$ ,  $\mathbf{t}_{o1}$  and  $\mathbf{t}_{o2}$  are denoted as B<sub>0</sub>, B<sub>1</sub> and B<sub>2</sub>, respectively. (b) The configurations of B<sub>1</sub> and B<sub>2</sub>. (c) The energy barrier and the evolution of out-of-plane polarization along the path in (a). The inset shows the identical magnetic configurations of B<sub>1</sub> and B<sub>2</sub>, where red and blue arrows denote opposite magnetic moments. (d) The two highest occupied bands of B<sub>1</sub> (left) and B<sub>2</sub> (right), calculated without considering SOC. The red and blue colors denote opposite spins. The Fermi level is set to zero. The inset displays the Brillouin zone, where the high symmetry points  $S_1 = (\frac{1}{2}, \frac{1}{2})$  and  $S_2 = (-\frac{1}{2}, \frac{1}{2})$ .

$\hat{O}_0 = \{m_{001}|(0.5, 0)\}$  and denoted as B<sub>0</sub>. B<sub>0</sub> is a high-symmetry state with the layer group  $pb2_1a$ , where the point group symmetry  $R^- = m_{001}$  enforces a zero  $P$  [Fig. 2(c)]. From the perspective of sliding-induced symmetry breaking, interlayer sliding of B<sub>0</sub> breaks  $m_{001}$  symmetry and induces  $P$  in B<sub>1</sub> (B<sub>2</sub>). Indeed, B<sub>1</sub> and B<sub>2</sub> are dual configurations connected by  $N^- = m_{001}$ , while B<sub>0</sub> is the self-dual configuration with  $m_{001}$  symmetry [57]. Hence, taking  $\mathbf{t}_{o0}$  as the origin,  $P$  as a function of interlayer translation  $\mathbf{t}_o$  is odd, while the energy as a function of translation is even, as shown in Fig. 2(c). The energy barrier for the ferroelectric switching from B<sub>1</sub> to B<sub>2</sub> is

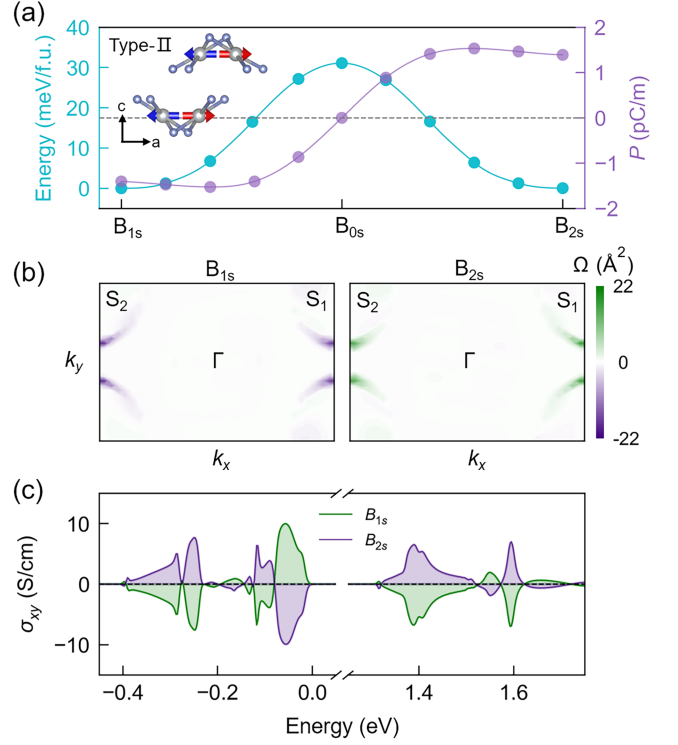


FIG. 3. (a) The energy barrier and the evolution of out-of-plane polarization between B<sub>1s</sub> and B<sub>2s</sub> along the same path as that between B<sub>1</sub> and B<sub>2</sub>. B<sub>0s</sub>, B<sub>1s</sub> and B<sub>2s</sub> refers to the bilayer B<sub>0</sub>, B<sub>1</sub> and B<sub>2</sub> under 4% biaxial tensile strain, respectively. The inset shows the identical magnetic configurations of B<sub>1s</sub> and B<sub>2s</sub>, where red and blue arrows denote the magnetic moment along [100] and  $\bar{[100]}$  directions, respectively. (b) The Berry curvatures of B<sub>1s</sub> and B<sub>2s</sub> in the first Brillouin zone. It is calculated by summing all the occupied states below 60 meV relative to the valence band maximum. (c) The anomalous Hall conductivities of B<sub>1s</sub> and B<sub>2s</sub>. The valence band maximum is set to zero.

17.1 meV/f.u.

In contrast to inversion symmetry breaking, stacking preserves the  $\{m_{100}|\frac{1}{2}, \frac{1}{2}\}$  symmetry for B<sub>1</sub> (B<sub>2</sub>) and thus inherits the altermagnetism, as shown in Fig. 2(d). The maximal spin splitting is 51 meV for the two highest occupied bands. We assume the magnetization direction of each atom remains unchanged under interlayer sliding. B<sub>1</sub> and B<sub>2</sub> with the type-I magnetic configuration are connected by  $N_s^- = \{2_\perp||m_{001}\}$ , which enforces them to have opposite  $\mathbf{k}$ -dependent spin polarizations [Fig. 2(d)]. We denote the energy splitting between the two spin channels at a certain  $\mathbf{k}$  point as  $\Delta E_{\mathbf{k}} = E_{\mathbf{k}}^\uparrow - E_{\mathbf{k}}^\downarrow$ . The intermediate state B<sub>0</sub> exhibits spin degeneracy enforced by its spin point group symmetry  $\{2_\perp||m_{001}\}$ . Taking  $\mathbf{t}_{o0}$  as the origin, similar to  $P$ ,  $\Delta E_{\mathbf{k}}$  as a function of interlayer translation is odd, as shown in Fig. S1 of the Supplemental Material [51]. Therefore, the spin polarization can be switched by sliding ferroelectricity in bilayer AgF<sub>2</sub>.

We next consider the SOC effect and discuss AHE in

$B_1$  and  $B_2$ . By comparing the energies of  $B_1$  ( $B_2$ ) with the Néel vector aligned along [100], [010] and [001] directions, we find that the easy axis is along the [100] direction, as shown in the inset of Fig. 2(c).  $B_1$  ( $B_2$ ) has the magnetic point group  $m' = \{1, m'_{100}\}$ , which permits a nonzero anomalous Hall conductivity  $\sigma_{xy}$ . However, considering SOC,  $B_1$  and  $B_2$  are connected by  $N_m^- = m_{001}$ , which does not switch the sign of Berry curvature and thus cannot switch the AHE. Switching AHE requires  $N_m^- = m'_{001}$ , which necessitates tuning the magnetic ground state of  $B_1$  ( $B_2$ ) to the type-II configuration, as shown in the inset of Fig. 3(a).

Strain is an efficient method to tune the magnetic phase [58–60]. We apply biaxial tensile strain to  $B_1$  and  $B_2$ , inducing a magnetic ground-state phase transition from type-I to type-II when the strain reaches or exceeds 3%, as detailed in Table S4 of the Supplemental Material [51]. We take  $\text{AgF}_2$  bilayers under a 4% biaxial tensile strain as an example, and denote  $B_{0s}$ ,  $B_{1s}$  and  $B_{2s}$  as the bilayer  $B_0$ ,  $B_1$  and  $B_2$  under strain, respectively. For both  $B_{1s}$  and  $B_{2s}$ , the type-II magnetic configuration is the ground state, with an energy 0.18 meV/f.u. lower than type-I. The easy axis remains along the [100] direction [see the inset of Fig. 3(a)]. While the sliding ferroelectricity is preserved under strain, as shown in Fig. 3(a).  $B_{1s}$  and  $B_{2s}$  exhibit opposite anomalous Hall conductivities as their connection operator  $N_m^- = m'_{001}$  reverses the sign of Berry curvature [see Figs. 3(b) and 3(c)]. The intermediate state  $B_{0s}$  exhibits a vanishing AHE, enforced by its magnetic point group symmetry  $m'_{001}$ . For the anomalous Hall conductivity at a fixed Fermi energy, taking  $t_{00}$  as the origin, its dependence on interlayer translation is odd, as a result of  $N_m^- = m'_{001}$  (see Fig. S2 in the Supplemental Material [51]). These results indicate that the AHE can be controlled by the sliding ferroelectricity in strained bilayer  $\text{AgF}_2$ .

*Summary and discussion.*— In summary, we propose a general rule for controlling unconventional magnetism, including altermagnetic spin splitting and AHE, via sliding ferroelectricity in bilayer systems. We reveal that the connection operator determines the magnetoelectric coupling, and identify all the possible altermagnetic bilayers that enable ferroelectric control of spin polarization or AHE. In fact, the general stacking rule is not only applicable to collinear altermagnets but also to non-collinear or noncoplanar spin configurations. Additionally, the rule can be extended beyond spin polarization and AHE to other spin-dependent properties that can be switched by the connection operator. Our work provides a general strategy for designing unconventional multiferroic bilayer systems and developing energy-efficient anti-ferromagnetic spintronic devices.

This work is supported by the National Key Research and Development Program of China (2022YFA1204100), the National Natural Science Foundation of China (62488201 and 12274194), Shenzhen Science and Tech-

nology Program (RCJC20221008092722009 and No. 20231117091158001), the Innovative Team of General Higher Educational Institutes in Guangdong Province (2020KCXTD001), and Guangdong Provincial Quantum Science Strategic Initiative (GDZX2401002).

\* [sxdu@iphy.ac.cn](mailto:sxdu@iphy.ac.cn)

† [liuqh@sustech.edu.cn](mailto:liuqh@sustech.edu.cn)

- [1] Q. Liu, X. Dai, and S. Blügel, Nat. Phys. (2025).
- [2] P. Liu, J. Li, J. Han, X. Wan, and Q. Liu, Phys. Rev. X **12**, 021016 (2022).
- [3] L. Šmejkal, J. Sinova, and T. Jungwirth, Phys. Rev. X **12**, 031042 (2022).
- [4] L. Šmejkal, J. Sinova, and T. Jungwirth, Phys. Rev. X **12**, 040501 (2022).
- [5] X. Chen *et al.*, Phys. Rev. X **14**, 031038 (2024).
- [6] Y. Jiang, Z. Song, T. Zhu, Z. Fang, H. Weng, Z.-X. Liu, J. Yang, and C. Fang, Phys. Rev. X **14**, 031039 (2024).
- [7] Z. Xiao, J. Zhao, Y. Li, R. Shindou, and Z.-D. Song, Phys. Rev. X **14**, 031037 (2024).
- [8] X. Chen, Y. Liu, P. Liu, Y. Yu, J. Ren, J. Li, A. Zhang, and Q. Liu, arXiv:2307.12366 **2307** (2023).
- [9] Y.-P. Zhu *et al.*, Nature **626**, 523 (2024).
- [10] J. Krempaský *et al.*, Nature **626**, 517 (2024).
- [11] L.-D. Yuan, Z. Wang, J.-W. Luo, E. I. Rashba, and A. Zunger, Phys. Rev. B **102**, 014422 (2020).
- [12] H.-Y. Ma, M. Hu, N. Li, J. Liu, W. Yao, J.-F. Jia, and J. Liu, Nat. Commun. **12**, 2846 (2021).
- [13] I. Mazin, K. Koepf, M. D. Johannes, R. Gonzalez-Hernandez, and L. Smejkal, Proc Natl Acad Sci U S A **118**, e2108924118 (2021).
- [14] S. Hayami, Y. Yanagi, and H. Kusunose, J. Phys. Soc. Jpn. **88**, 123702 (2019).
- [15] L. Šmejkal, R. González-Hernández, T. Jungwirth, and J. Sinova, Sci. Adv. **6**, eaaz8809 (2020).
- [16] M. Naka, S. Hayami, H. Kusunose, Y. Yanagi, Y. Motome, and H. Seo, Nat. Commun. **10**, 4305 (2019).
- [17] R. Gonzalez-Hernandez, L. Smejkal, K. Vyborny, Y. Yahagi, J. Sinova, T. Jungwirth, and J. Zelezny, Phys. Rev. Lett. **126**, 127701 (2021).
- [18] M. Naka, Y. Motome, and H. Seo, Phys. Rev. B **103**, 125114 (2021).
- [19] H. Bai *et al.*, Phys. Rev. Lett. **128**, 197202 (2022).
- [20] D. F. Shao, S. H. Zhang, M. Li, C. B. Eom, and E. Y. Tsymlal, Nat. Commun. **12**, 7061 (2021).
- [21] L. Šmejkal, A. B. Hellenes, R. González-Hernández, J. Sinova, and T. Jungwirth, Phys. Rev. X **12**, 011028 (2022).
- [22] L. Bai, W. Feng, S. Liu, L. Šmejkal, Y. Mokrousov, and Y. Yao, Adv. Funct. Mater. **34**, 2409327 (2024).
- [23] L. Šmejkal, A. H. MacDonald, J. Sinova, S. Nakatsuji, and T. Jungwirth, Nat. Rev. Mater. **7**, 482 (2022).
- [24] N. Nagaosa, J. Sinova, S. Onoda, A. H. MacDonald, and N. P. Ong, Rev. Mod. Phys. **82**, 1539 (2010).
- [25] H. Chen, Q. Niu, and A. H. MacDonald, Phys. Rev. Lett. **112**, 017205 (2014).
- [26] J. Kübler and C. Felser, EPL (Europhysics Letters) **108**, 67001 (2014).
- [27] S. Nakatsuji, N. Kiyohara, and T. Higo, Nature **527**, 212 (2015).

- [28] A. K. Nayak *et al.*, *Sci. Adv.* **2**, e1501870.
- [29] M. T. Suzuki, T. Koretsune, M. Ochi, and R. Arita, *Phys. Rev. B* **95**, 094406 (2017).
- [30] T. Jungwirth, X. Marti, P. Wadley, and J. Wunderlich, *Nat. Nanotechnol.* **11**, 231 (2016).
- [31] V. Baltz, A. Manchon, M. Tsoi, T. Moriyama, T. Ono, and Y. Tserkovnyak, *Rev. Mod. Phys.* **90**, 015005 (2018).
- [32] P. Wadley *et al.*, *Science* **351**, 587 (2016).
- [33] L. Han *et al.*, *Sci. Adv.* **10**, eadn0479 (2024).
- [34] E. Y. Tsymbal, *Nat. Mater.* **11**, 12 (2011).
- [35] J. F. Scott, *Nat. Mater.* **6**, 256 (2007).
- [36] K. L. Wang, J. G. Alzate, and P. Khalili Amiri, *J. Phys. D: Appl. Phys.* **46**, 074003 (2013).
- [37] W. Sun, W. Wang, C. Yang, R. Hu, S. Yan, S. Huang, and Z. Cheng, *Nano Lett.* **24**, 11179 (2024).
- [38] L. Li and M. Wu, *ACS Nano* **11**, 6382 (2017).
- [39] J. Ji, G. Yu, C. Xu, and H. Xiang, *Phys. Rev. Lett.* **130**, 146801 (2023).
- [40] R. He, D. Wang, N. Luo, J. Zeng, K. Q. Chen, and L. M. Tang, *Phys. Rev. Lett.* **130**, 046401 (2023).
- [41] B. Pan, P. Zhou, P. Lyu, H. Xiao, X. Yang, and L. Sun, *Phys. Rev. Lett.* **133**, 166701 (2024).
- [42] Y. Liu, J. Yu, and C.-C. Liu, *Phys. Rev. Lett.* **133**, 206702 (2024).
- [43] S. Zeng and Y.-J. Zhao, *Phys. Rev. B* **110**, 174410 (2024).
- [44] C. Bradley and A. Cracknell, *The mathematical theory of symmetry in solids: representation theory for point groups and space groups* (Oxford University Press, 2010).
- [45] W. Brinkman and R. J. Elliott, *Proceedings of the Royal Society of London. Series A. Mathematical and Physical Sciences* **294**, 343 (1966).
- [46] W. Brinkman and R. J. Elliott, *J. Appl. Phys.* **37**, 1457 (1966).
- [47] D. B. Litvin and W. Opechowski, *Physica* **76**, 538 (1974).
- [48] Y. Zhu, J.-T. Sun, J. Pan, J. Deng, and S. Du, *Phys. Rev. Lett.* **134**, 046403 (2025).
- [49] D.-F. Shao, J. Ding, G. Gurung, S.-H. Zhang, and E. Y. Tsymbal, *Phys. Rev. Appl.* **15**, 024057 (2021).
- [50] T. Cao, D.-F. Shao, K. Huang, G. Gurung, and E. Y. Tsymbal, *Nano Lett.* **23**, 3781 (2023).
- [51] See Supplemental Material for details about group theory analysis, computational methods and the DFT results of altermagnetic bilayer AgF<sub>2</sub>.
- [52] J. S odequist and T. Olsen, *Appl. Phys. Lett.* **124**, 182409 (2024).
- [53] S. Zeng and Y.-J. Zhao, *Phys. Rev. B* **110**, 054406 (2024).
- [54] Y. Liu, J. Li, and Q. Liu, *Nano Lett.* **23**, 8650 (2023).
- [55] P. Fischer, D. Schwarzenbach, and H. M. Rietveld, *J. Phys. Chem. Solids* **32**, 543 (1971).
- [56] X. Xu, Y. Ma, T. Zhang, C. Lei, B. Huang, and Y. Dai, *Nanoscale Horiz.* **5**, 1386 (2020).
- [57] M. Fruchart, Y. Zhou, and V. Vitelli, *Nature* **577**, 636 (2020).
- [58] Y. Qi, M. A. Sadi, D. Hu, M. Zheng, Z. Wu, Y. Jiang, and Y. P. Chen, *Adv. Mater.* **35**, 2205714 (2023).
- [59] J. Cenker *et al.*, *Nat. Nanotechnol.* **17**, 256 (2022).
- [60] A. M. Le on, J. W. Gonz alez, J. Mej ia-L pez, F. Crasto de Lima, and E. Su arez Morell, *2D Mater.* **7**, 035008 (2020).